Hindawi
Journal of Chemistry
Volume 2023, Article ID 9828402, 1 page
https://doi.org/10.1155/2023/9828402

Retraction

Retracted: Monitoring of Nitrogen Transport Data in Pear Leaves Based on Infrared Spectroscopy

Journal of Chemistry

Received 15 August 2023; Accepted 15 August 2023; Published 16 August 2023

This article has been retracted by Hindawi following an investigation undertaken by the publisher [1]. This investigation has uncovered evidence of one or more of the following indicators of systematic manipulation of the publication process:

(1) Discrepancies in scope

(2) Discrepancies in the description of the research reported

(3) Discrepancies between the availability of data and the research described

(4) Inappropriate citations

(5) Incoherent, meaningless and/or irrelevant content included in the article

(6) Peer-review manipulation

The presence of these indicators undermines our confidence in the integrity of the article's content and we cannot, therefore, vouch for its reliability. Please note that this notice is intended solely to alert readers that the content of this article is unreliable. We have not investigated whether authors were aware of or involved in the systematic manipulation of the publication process.

Wiley and Hindawi regrets that the usual quality checks did not identify these issues before publication and have since put additional measures in place to safeguard research integrity.

We wish to credit our own Research Integrity and Research Publishing teams and anonymous and named external researchers and research integrity experts for contributing to this investigation.

The corresponding author, as the representative of all authors, has been given the opportunity to register their agreement or disagreement to this retraction. We have kept a record of any response received.

References

[1] Z. Fan, D. Wang, and N. Zhang, "Monitoring of Nitrogen Transport Data in Pear Leaves Based on Infrared Spectroscopy," *Journal of Chemistry*, vol. 2022, Article ID 1547582, 9 pages, 2022.

Hindawi
Journal of Chemistry
Volume 2022, Article ID 1547582, 9 pages
https://doi.org/10.1155/2022/1547582

Research Article

Monitoring of Nitrogen Transport Data in Pear Leaves Based on Infrared Spectroscopy

Zehua Fan,[1] **Desheng Wang**,[2] **and Nannan Zhang**[1]

[1]*College of Information Engineering, Tarim University, Alar, Xinjiang 843300, China*
[2]*College of Plant Sciences, Tarim University, Alar, Xinjiang 843300, China*

Correspondence should be addressed to Zehua Fan; 2013071225@stu.zjhu.edu.cn

Received 19 April 2022; Revised 19 May 2022; Accepted 25 May 2022; Published 7 June 2022

Academic Editor: Aruna K K

In order to better monitor the data of nitrogen transport in pear leaves, a method based on infrared spectroscopy was proposed. The near-infrared reflection spectrum imaging technology is used to collect the leaf scale spectral image of the target crop. Computer image analysis software is used to process the spectral digital image and extract the spectral data. After statistical analysis, the data are selected as variables. Combined with the chemical analysis test results, the crop nutrition detection model is established, and the conclusion is drawn. The experimental results show that the band gray data involved in the model are scaled and reorganized according to the coefficient proportion by using ENVI through the band calculation command. The final gray image, the original image, and the gray image in the process default to the three-channel analog image of the band (the wavelengths of the bands are 1446, 1373, and 1304 nm, respectively); 944 nm gray image; 1043 nm gray scale image; 1662 nm gray image; $(0.102R_{944} + 0.103R_{1\ 043} + 0.206R_{1662})/(0.102 + 0.103 + 0.206)$ grayscale image with signal scaling according to the scale of model coefficient. It is proved that infrared spectroscopy can effectively monitor the data of nitrogen transport in pear leaves.

1. Introduction

Each substance has different absorption, reflection, and transmission of electromagnetic waves of different wavelengths (or frequencies). This response characteristic of substances to the spectra of different bands is called the spectral characteristic. Nondestructive monitoring of the crop nitrogen nutrition spectrum is based on the characteristic response of different nitrogen forms in crop leaves or other organs and tissues to different spectral bands. Using the remote sensing sensor to obtain the characteristic spectral information of crops without damaging the tissue structure of crops or far away from crops, and analyze and process these information, so as to judge the deficiency degree of nitrogen nutrition and quantitatively retrieve the status of nitrogen nutrition of crops [1]. The spectral monitoring principle of crop nitrogen nutrition is that the chemical bonds in the molecular structures of various protein nitrogen, amino acids, chloroplasts, and other nitrogen components in crop tissue vibrate under the irradiation of light energy at a certain radiation level (different frequencies or wavelengths), resulting in differences in absorption and reflection of light at some wavelengths, forming different reflection, absorption, and transmission spectra. The changes of spectral reflectance in these bands are abnormally sensitive to the number of specific nitrogen components, which is called nitrogen band or sensitive spectrum [2]. The band range of the response of the main nitrogen forms in crops is concentrated in the visible and infrared regions. The former is the electron transition spectrum, and the latter is the molecular vibration spectrum. When these different energy lights irradiate crops with different nitrogen nutritional status, they produce characteristic nitrogen reflection and absorption spectrum. The realization of crop nitrogen nutrition spectrum monitoring is based on the quantitative relationship between the sensitive reflection spectrum or absorption spectrum of the crop nitrogen component and the content or concentration of the component [3].

The traditional methods of crop nitrogen diagnosis are qualitative and semiquantitative methods based on conventional indoor chemical quantitative analysis, seedling

fertilization, leaf color card, and so on. The former judges whether the crop is short of nitrogen by the nitrogen content of the crop plant (or leaf), starch content of the leaf sheath, nitrate nitrogen at the base of the stem, amino nitrogen content of the functional leaf or leaf sheath, and C/N ratio of the leaf [4]. Although this method is intuitive and reliable, it is difficult to be applied in time, generally, because of its destructive large number of samples, which leads to time-consuming, labor-consuming, and high-analysis cost. Although the latter is more intuitive and fast, it lacks quantitative diagnostic indicators, which are not conducive to accurately estimate the amount of nitrogen fertilizer. In recent years, the multispectral and hyperspectral remote sensing technology based on the spectral characteristics of ground objects has developed rapidly, which makes it possible to obtain the crop growth status and plant biochemical components in real time, fast, accurate, large-scale, and nondestructive means, thus providing a new technical means and method for the nondestructive monitoring of crop growth. This is because crop nitrogen deficiency will cause a series of changes in leaf color, thickness, and morphological structure, resulting in changes in spectral absorption, reflection, and transmission characteristics, which provides a theoretical basis for real-time monitoring and rapid diagnosis of crop nitrogen status based on spectral reflection characteristics [5].

The canopy color of crops is directly affected by the change of nutritional status. The leaf color of nitrogen deficient plants becomes lighter, and the canopy color is yellow and green. In this way, after the canopy image is obtained and processed by the computer program, the red light (R), green light (G), and blue light (B) reflected by plant canopy can be accurately quantified for nitrogen nutrition diagnosis. In recent years, more and more studies have been carried out to understand the nitrogen nutrition status of crops by judging the color depth of crop canopy or to recommend fertilization and predict yield [6]. Visible light color analysis technology has become a new research hot spot. In these studies, researchers mostly use the relative value of canopy image color or the ratio G/R of canopy green light reflection to red light reflection to diagnose nitrogen nutrition. Samadi and others predicted maize yield by analyzing the relative brightness of canopy on color photos. There was a very significant correlation between the red, green, and blue light and the maize yield [7]. Jani and others obtained the canopy image of winter wheat with a digital camera, analyzed the ratio of green light to red light in the canopy image, and considered that there was a very significant correlation between G/R and chlorophyll meter reading [8]. Fan showed that there was a good linear positive correlation between the relative green and blue depth values of canopy images from 6-leaf stage to 7-leaf stage and the optimal economic nitrogen application rate [9]. Au established the relationship model between canopy green depth and above ground plant total nitrogen at jointing stage and booting stage by using a digital camera. These research works lay a foundation for the application of color image processing technology based on digital camera and machine vision color recognition technology in crop growth monitoring. However, there is little research in this field, and there is no consistent image acquisition and processing standard [10]. Therefore, the use of canopy color analysis for nitrogen nutrition diagnosis needs to be further studied. Wang Y. believes that changes in the contents of nitrogen, phosphorus, and potassium in crops will cause changes in the physiological and morphological structure of crop leaves and the spectral reflection characteristics of crops. This is the theoretical basis for obtaining crop nutrient information through spectral remote sensing, making it possible to diagnose the nutritional status in the field nondestructively, quickly, and simply [11]. Veeravu believes that the traditional remote sensing monitoring technology based on multispectral and broadband reflectance has made some progress. However, due to its few spectral bands and low resolution, it is easy to lead to the lack of some key spectral information [12]. Alwi believes that in recent years, the emergence and rise of hyperspectral remote sensing technology can subdivide the spectral band in a specific spectral region with its characteristics of high resolution, continuous band, and abundant data, which has injected new vitality into the nutrition diagnosis of crops [13]. Koroleva research on vegetation spectral repression monitoring has made some progress in the scales of dry powder, fresh leaf canopy, and aviation, which proves the feasibility of spectral remote sensing analysis technology for crop nitrogen nutrition diagnosis [14]. Using hyperspectral remote sensing technology, Estak I. can quickly and accurately obtain all kinds of information about crop growth status and environmental stress, so as to guide the corresponding management measures and the amount of input materials, so as to reduce waste, increase yield, and protect agricultural resources and environmental quality. It is an important means for the sustainable development of precision agriculture and agriculture in the future [15]. Andrade C. A. believes that hyperspectral remote sensing has the characteristics of high spectral resolution (band width <10 nm), strong band continuity (hundreds of bands in the range of 400~2500 mm), large amount of spectral information, and so on. It can simultaneously obtain continuous spectral images of ground objects with high spectral resolution in a specific spectral domain. The gray value of each pixel point in each channel on the spectral image can form a fine spectral line, which can form a unique ultra multidimensional spectral space, so that remote sensing applications focus on spatial information expansion in the spectral dimension to obtain more fine spectral information and provide parameters and basis for quantitative analysis of the physical and chemical change process of surface materials [16].

Based on the current research, a method based on infrared spectroscopy is proposed in this paper. The near-infrared reflectance spectral imaging technology is used to collect the leaf scale spectral image of the target crop, and the computer image analysis software is used to process the spectral digital image and extract the spectral data. The near-infrared reflectance hyperspectral imaging system is shown in Figure 1. After statistical analysis, the data are selected as variables, and the crop nutrition detection model is established in combination with the chemical analysis test results. The conclusion is drawn from the test model.

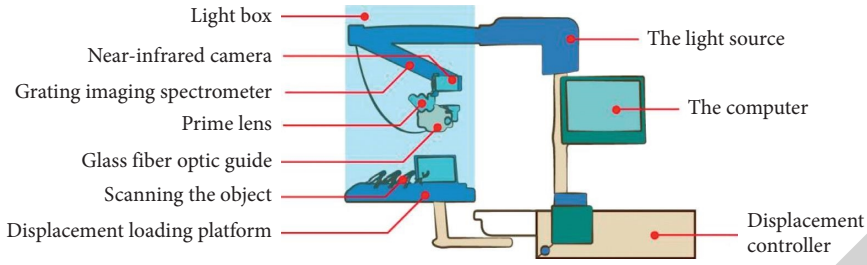

Figure 1: Hyperspectral image acquisition system.

2. Materials and Methods

2.1. Sample Selection and Collection. In the experiment, the leaves of the self-cultivated pear tree (the variety is pear tree: Hanyu seed industry, produced by the experimental field of the 6th regiment of the first division in southern Xinjiang) were selected as the test samples. In order to obtain the test samples with different levels of nutrient content, the nutrient supply in the process of crop cultivation adopts the uniform design of lack stress treatment. 9 groups A-I of the standard nutrient supply formula, 20%, 30%, 40%, 50%, 60%, 70%, 80%, 90%, and 100%, are taken as the actual nutrient supply level of the test samples. One group of control group O was arranged according to the standard nutrition supply formula. The number of sample plants in each experimental group and control group was 8. The other cultivation conditions except for nutrition supply were suitable, and the growth environment was the same.

After enough time of cultivation and nutrient stress treatment, the test samples were selected in the critical period of pear nutrition when most individuals have changed from vegetative growth stage to reproductive growth stage. Four plants in each group who have completed the excessive growth stage were randomly selected, and the 5th, 6th, and 7th true leaves were completely picked. The picked leaves were placed in fresh-keeping bags for temporary storage, and attention was paid to keeping them away from light. The time from leaf picking to the spectrum acquisition test shall not exceed 1 h [17].

2.2. Spectrum Acquisition Equipment and Test. In order to obtain all the near-infrared spectrum information on each crop leaf, the reflection hyperspectral scanning system (Inspector VIOE, Finland) is selected to collect the reflection spectrum information in the near-infrared region (900–1700 nm) of each leaf to be tested. The near-infrared reflection hyperspectral imaging system is shown in Figure 1.

The system is mainly composed of the near-infrared camera, grating imaging spectrometer, *f*/2.0 fixed focus lens, 150 W tungsten halogen lamp DC adjustable light source, glass fiber light guide, step displacement stage, step controller, and computer. The spatial resolution of the detection system is very high, and it can recognize the fine distance within 15 nm. The field resolution of its near-infrared camera is 320×256 (pixels). The spectral information collected by it contains the near-infrared reflection intensity of 872–1766 nm. This wide-range band is divided into 256 narrow-range bands: band 1-band 256, the spectral resolution is 5 nm, and the width of the illumination slit scanned by a single exposure is 30 μM. The distance between the spectrum detection camera and the stage is about 25 cm. Before hyperspectral data acquisition, turn on the light source to preheat the machine for more than 30 rain. The exposure time of the camera is set to 20 ms, and the speed of moving the stage is 1 mm/s [18]. After the preparation of black-and-white field calibration through equipment control software, near-infrared reflection hyperspectral imaging scanning was carried out one by one for three leaf samples of four individuals in each group, having a total of 120 samples, and the spectral information acquisition was completed.

2.3. Chemical Determination of Total Nitrogen Content in Sample Leaves. Complete the spectral data acquisition. The leaves of pear tree samples were treated immediately for subsequent chemical analysis. The total nitrogen content of the solution to be measured was measured after the leaves were treated with auto analyzer 3 (later abbreviated as aa3) continuous flow analyzer produced by German seal, such as killing, drying, grinding, screening, digestion, filtration, and constant volume. Each time the aa3 flow analyzer is used, it shall be noted that the process of starting up, preheating, running, and reading the baseline shall not be less than 1 h, so as to ensure that the machine is preheated completely, and the analysis is accurate. In order to obtain enough samples to complete the acquisition of the liquid to be tested, evenly mix the sample powder obtained after grinding and screening the three blades of four individuals in each group, weigh about 0.1 g for subsequent operation, that is, only one sample of the liquid to be tested in each group is obtained for chemical analysis and determination [19].

2.4. Remote Sensing Image Processing. Use formulas (1) and (2) to calculate the first-order guided etching of spectral reflectance, and determine the position, slope (amplitude), and area of blue edge, yellow edge, and red edge in the range of 490~530 nm, 550~582 nm, and 680~750 nm, respectively. The position of red edge is the wavelength corresponding to the maximum value of first-order derivative spectrum in the range of red light, the slope of red edge is the maximum value of first-order derivative spectrum of reflectance, and the area of red edge is the area surrounded by the spectral line of first-order derivative of reflectance. The yellow and

blue edge parameters have similar meanings to the red edge parameters. The above parameters can be combined through difference, ratio, and normalized difference processing. In addition, referring to the characteristics of trilateral parameters, the maximum value and corresponding wavelength of the first derivative of reflectance in the near-infrared range of 920–980 nm, 1000–1060 nm, and 1100 ~ 1180 nm are calculated [20].

$$R'(\lambda_i) = \frac{dR(\lambda_i)}{d\lambda} = \frac{R(\lambda_{i+1}) - R(\lambda_{i-1})}{2\Delta\lambda}, \quad (1)$$

$$R(\lambda_i) = \frac{dR(\lambda_i)}{d\lambda} = \frac{R(\lambda_{i+1}) - R(\lambda_{i-1})}{2\Delta\lambda}. \quad (2)$$

The red edge parameters can also be obtained by the anti-Gaussian red edge optical model (IG model). IG model suggests that the red edge (670–800 nm) reflection spectrum curve can be fitted with an inverse Gauss model (formula 3):

$$R(\lambda) = R_s - (R_s - R_0)\exp\left(\frac{-(\lambda_0 - \lambda)^2}{2\sigma^2}\right), \quad (3)$$

where R_s is the shoulder reflection value (maximum reflectivity) in the near-infrared region, R_0 is the minimum reflectivity in the red light region, λ_0 is the wavelength corresponding to R_0, σ is the standard deviation coefficient of Gaussian function, which is also the difference between the red edge spectral position of vegetation feature spectrum and the Red Valley spectral position, and corresponds to the width of the red edge absorption valley [21].

In this paper, the average value of spectral reflectance in the range of 670–675 nm is defined as R_0, and the average value of spectral reflectance in the range of 780–795 nm is defined as R_s. The reflectance in the range of 685–780 nm is selected as the object of inverse Gaussian model simulation. The reflectance spectrum at the red edge of wheat is logarithmically transformed using two parameters, R_0 and R_s, as shown in the following formula:

$$B(\lambda) = \left[-\ln\frac{R_s - R(\lambda)}{R_s - R_0}\right]^{1/2}, \quad (4)$$

where $B(\lambda)$ is the value after logarithmic transformation of wheat red edge reflectance spectrum. By linear fitting $B(\lambda)$ and λ, the slope a_1 and intercept a_0 can be obtained. Then, the Red Valley spectral position and absorption valley width λ_0 and σ are, respectively, as shown in the following formulas:

$$\lambda_0 = -\frac{a_0}{a_1}, \quad (5)$$

$$\sigma = \frac{1}{\sqrt{2a_1}}. \quad (6)$$

In this study, a new spectral index of nitrogen in the leaf layer of pear tree was constructed, and the algorithm with a large number of spectral parameters was synthesized and programmed in the MATLAB language environment. Comprehensive independent experiments were conducted to analyze the correlation between leaf layer nitrogen nutrition and growth indexes, spectral reflectance, and characteristic spectral parameters in different growth stages, select the appropriate spectral index sensitive to agronomic indexes, establish the monitoring model, and further test, verify, and improve the model by using the experimental data of independent years [22].

At the same time, the relationship between the spectral ratio index (SR), normalization index (ND), and difference index (DI) combined by any two bands in the range of 350.2500 nm and leaf layer nitrogen status (equations (7)–(9)) was systematically studied in order to find the best band combination parameters for predicting pear leaf pigment content. MATLAB was used to display the equipotential diagram of the determination coefficient between the 2-band vegetation index and leaf nitrogen status.

$$SR(R_{\lambda1}, R_{\lambda2}) = \frac{R_{\lambda1}}{R_{\lambda2}}, \quad (7)$$

$$ND(R_{\lambda1}, R_{\lambda2}) = \frac{|R_{\lambda1} - R_{\lambda2}|}{R_{\lambda1} + R_{\lambda2}}, \quad (8)$$

$$DVI(R_{\lambda1}, R_{\lambda2}) = R_{\lambda1} - R_{\lambda2}. \quad (9)$$

The model is comprehensively evaluated by three general indexes: root mean square difference (RMSE), relative error (RE), and accuracy (R^2).

3. Experimental Results and Analysis

3.1. Data Analysis of Total Nitrogen Content in Sample Leaves. The data obtained through aa3 chemical analysis are the three detection values of NH_4^+ concentration in the solution to be measured, which are averaged and expressed by AVE. According to formula (1), the percentage content of total nitrogen in the leaves of each group of pear tree samples can be obtained, as shown in the following formula:

$$N(\%) = \frac{AVE\left(M_N/M_{NH_4^+}\right)V}{m} \times 100\%, \quad (10)$$

where $N(\%)$ is the percentage of total nitrogen; AVE is the average value of three repetitions of machine measurement; M_N is the atomic weight of nitrogen; NH_4^+ is the relative mass of ammonium ion; V is the volume of liquid to be measured after digestion, filtration and constant volume; and M is the dry matter mass of the blade.

The calculation results are arranged from small to large, as shown in Figure 2.

Through the above analysis and the results obtained, it can be seen that with the above culture scheme, the nitrogen nutrition level of pear trees has indeed been properly opened, which is reflected in a certain gradient in the total nitrogen content of leaves [23].

3.2. Analysis of Reflection Spectrum Data of the Sample Blade. The data collected by hyperspectral imaging scanning system is actually a four-dimensional data set containing two plane dimensions of spatial information, radiation wavelength

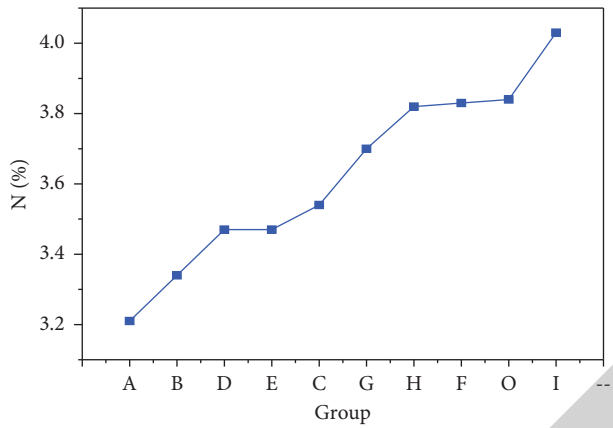

Figure 2: Percentage content of total nitrogen in leaves of 10 groups of samples.

information, and intensity information. In the study, ENVI 4.5 (Exelis visual information solutions, USA) was used to process and analyze the data set, and the special ROI (region of interest) selection command in software was used to quickly select all pixels constituting the leaf pattern of the target sample, so as to directly eliminate the information interference of the background pixels.

ENVI can quickly analyze the selected ROI, eliminate the spectral data that the computer considers to be abnormal points through statistical analysis, and directly establish the mean spectral curve with the screened data, and the spectral average reflectance curve of each group of 12 leaf samples can be simply drawn by using the spectral calculation command. The near-infrared reflectance mean spectral curve of 10 groups of leaf samples is shown in Figure 3, in which ε, λ are reflectance and wavelength, respectively [24].

The spectral reflection data of the near-infrared reflectance mean curve of 10 groups of leaf samples are derived by software. Each group of leaf samples has the gray value of 256 bands corresponding to the wavelength. Taking the gray $R_i (i = 1, 2, \ldots, 256)$ at each wavelength as the independent variable, the univariate linear regression is carried out for the dependent variable IV (%) one by one. There are 142 groups of regression determination coefficients $R^2 > 0.8$, and when retaining 3 decimal places, the minimum significance level of the original hypothesis is rejected in the model test, $P = 0.000$. This shows that the 142 band gray data is statistically significant to reflect the percentage of total nitrogen.

Figure 4 shows the univariate regression R^2 of gray level of each band to leaf nitrogen content. According to the variation trend of R^2 with wavelength in the figure, 142 bands with R^2 reaching 0.8 are divided into 6 regions and named according to the trend: B15-B21 (932~957 nm) is the "reliable near peak band;" B22-B46 (961–1054 am) is the "stable response band;" B47—B72 (1 058–1147 nm) is the "reliability fluctuation rising band;" B73-B103 (1 150~1 250 nm) is the "reliable peak band;" B104-B142 (1 253–1 373 AM) is the "reliability fluctuation decline band;" B219-B232 (1 626~1 673 nm) is the "reliable far peak band."

Due to the continuity of spectral data, in theory, there should be multiple collinearities between the gray levels of bands close to each other. Therefore, the collinearity diagnosis of spectral data in each region is carried out. The methods include correlation coefficient (r) analysis and the variance expansion factor (VIF) test. Taking the I region as an example, the test results are shown in Figures 5 and 6; R^2 in the table is the spectral reflectance at this i wavelength.

Figure 5 shows that the correlation coefficient r is higher than 0.9, the minimum is 0.968, and the maximum is 0.999, indicating that the correlation between gray levels in the first region of the band is very strong.

It can be seen from Figure 6 that the swelling of 7 variables is significantly higher than 10, so it can be considered that there is a serious multicollinearity between 6 gray levels in region 1. Using the above test method to test the collinearity of gray levels in other band regions, the results are similar, and the closer the band is, the more obvious the multicollinearity is [25].

In order to extract more useful information and avoid the influence of the multicollinearity between known spectral data in close bands as far as possible, the bands with the highest R2 regressed with total nitrogen content were selected from six regions, namely, B18 (944 nm), B43 (1043 nm), B72 (1147 nm), B87 (1198 nm), B104 (1253 nm), and B229 (1662 nm).

However, further research shows that when only R_{1043} and R_{1662} : 2 variables are retained, the estimated value of the ridge trace display coefficient will no longer tend to be stable with the increase of K, as shown in Figure 7.

When only R_{1043} and R_{1662} 2 variables are retained, the coefficient ridge estimation shows a rising trend as k increases, which does not tend to be stable, that is, there is a large deviation between the coefficient estimation and the real value. This shows that it is not appropriate to retain only two variables to establish the prediction model of nitrogen content in pear leaves.

The R^2 and F values are adjusted by the comprehensive determination coefficient, and the finally selected band gray levels are R_{994}, R_{1043}, and R_{1662}. The best prediction model of total nitrogen content in pear leaves is established by ridge regression, as shown in the following formula:

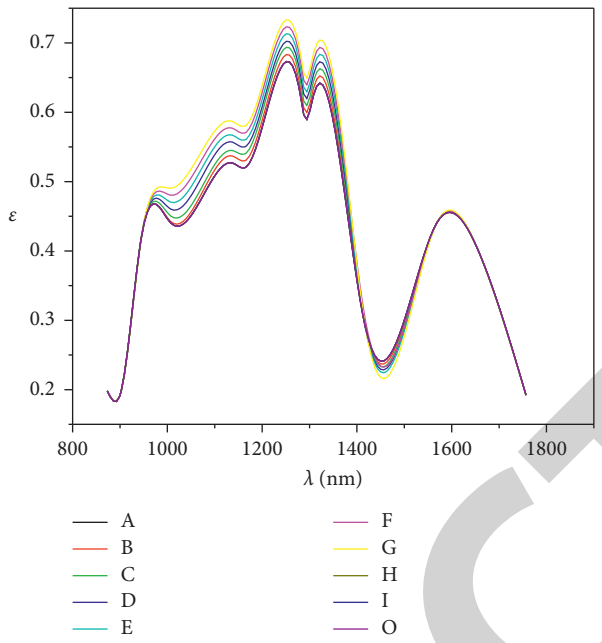

Figure 3: Near-infrared mean reflectance spectrum curve.

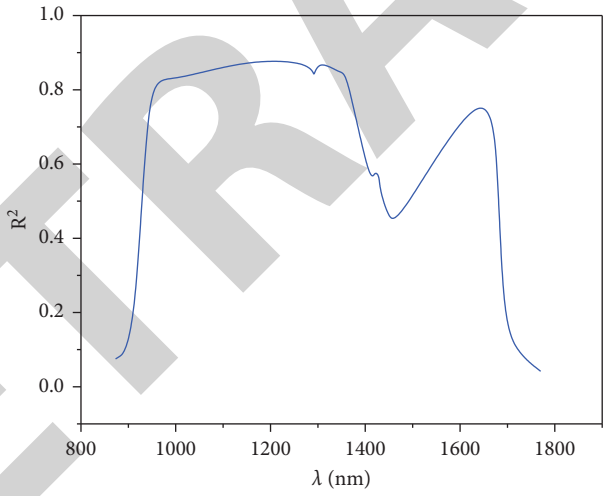

Figure 4: Univariate regression R^2 of gray level of each band on leaf nitrogen content.

$$N(\%) = -0.102R_{944} - 0.103R_{1043} - 0.206R_{1662} + 20.425. \quad (11)$$

The adjusted R^2 of the prediction model is 0.843, and the root mean square error RMSE is 0.105.

Use ENVI to scale and reorganize the band gray data involved in the model according to the coefficient proportion through the band calculation command. The final gray image, the original image, and the gray image in the process default to the 3-channel analog image of the band (the wavelengths of the bands are 1446, 1373, and 1304 nm, respectively); 944 nm gray image; 1043 nm grayscale image; 1662 nm gray image; and $(0.102R_{944} + 0.103R_{1043} + 0.206R_{1662})/(0.102 + 0.103 + 0.206)$ gray scale image are scaled by the model coefficient.

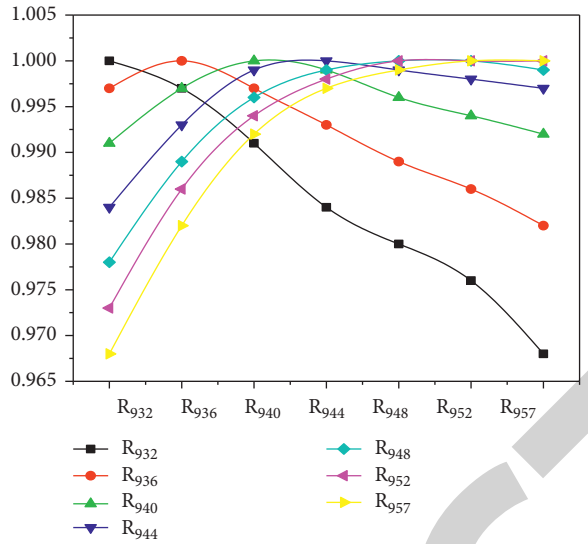

Figure 5: Correlation coefficient between gray values in the first region of the band.

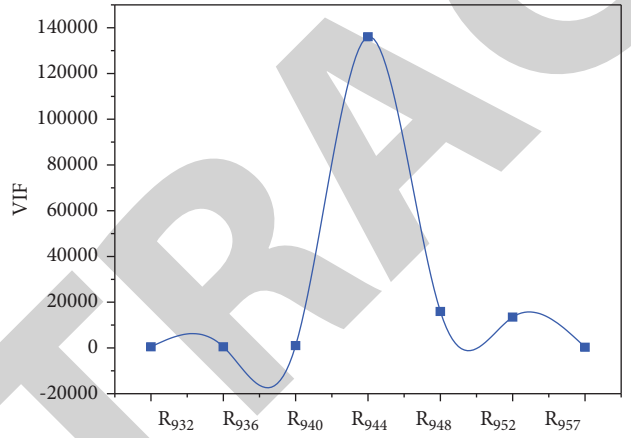

Figure 6: VIF test results of the gray value in the first region of band 4.

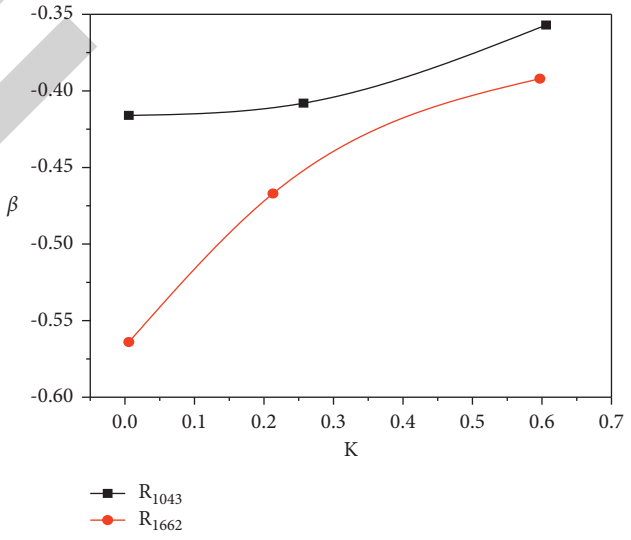

Figure 7: 2-variable ridge trace diagram.

4. Conclusion

Through the experimental operation and data analysis, based on the near-infrared reflection spectrum data and using ridge regression to screen the variables, a set of spectral detection model suitable for the total nitrogen content of pear leaves is finally obtained. The adjustment R^2 of the model is > 0.8, which shows that the fitting effect of the regression model is good, and the root mean square error RMSE is about 0.1, which shows that the model has high prediction accuracy. The model contains the spectral reflectance data of three near-infrared short wave characteristic bands, and the available information is more comprehensive.

Data Availability

The data used to support the findings of this study are available from the corresponding author upon request.

Conflicts of Interest

The authors declare that they have no conflicts of interest.

References

[1] J. Huang, M. Li, H. Zhang et al., "Using near infrared spectroscopy to quickly analyze different nitrogens during the shortcut biological removal of nitrogen from a polluted river," *Polish Journal of Environmental Studies*, vol. 28, no. 4, pp. 2623–2631, 2019.

[2] L. S. Wang, R. J. Wang, C. P. Lu, J. Wang, and L. T. Song, "Quantitative analysis of total nitrogen content in monoammonium phosphate fertilizer using visible-near infrared spectroscopy and least squares support vector machine," *Journal of Applied Spectroscopy*, vol. 86, no. 3, pp. 465–469, 2019.

[3] J. Liu, N. Li, F. Zhen, Y. Xu, W. Li, and Y. Sun, "Rapid detection of carbon-nitrogen ratio for anaerobic fermentation feedstocks using near-infrared spectroscopy combined with bipls and gsa," *Applied Optics*, vol. 58, no. 18, p. 5090, 2019.

[4] M. A. Hossen, P. K. Diwakar, and S. Ragi, "Total nitrogen estimation in agricultural soils via aerial multispectral imaging and libs," *Scientific Reports*, vol. 11, no. 1, Article ID 12693, 2021.

[5] L. Dan, Z. Huang, S. Men, and C. Wang, "Nitrogen and phosphorus adsorption in aqueous solutions by humic acids from weathered coal: isotherm, kinetics and thermodynamic analysis," *Water Science and Technology*, vol. 79, no. 11, pp. 2175–2184, 2019.

[6] H. Zhou, S. Gao, W. Zhang, Z. An, and D. Chen, "Dynamic adsorption of toluene on amino-functionalized sba-15 type spherical mesoporous silica," *RSC Advances*, vol. 9, no. 13, pp. 7196–7202, 2019.

[7] S. Wajizah and Z. Zulfahrizal, "Near infrared spectra features of cocoa pod husk used for feedstuff," *IOP Conference Series: Earth and Environmental Science*, vol. 922, no. 1, Article ID 012011, 2021.

[8] H. F. Ahmad Jani, R. Meder, H. A. Hamid, S. M. Razali, and K. H. M. Yusoff, "Near infrared spectroscopy of plantation forest soil nutrients in sabah, Malaysia, and the potential for microsite assessment," *Journal of Near Infrared Spectroscopy*, vol. 29, no. 3, pp. 148–157, 2021.

[9] Y. Fan, H. Wang, L. Deng et al., "Enhanced adsorption of pb(ii) by nitrogen and phosphorus co-doped biochar derived from camellia oleifera shells," *Environmental Research*, vol. 191, no. 26, Article ID 110030, 2020.

[10] J. Au, K. N. You Nge Ntob, W. J. Foley, B. D. Moore, T. Fea Rn, and J. Au, "Sample selection, calibration and validation of models developed from a large dataset of near infrared spectra of tree leaves," *Journal of Near Infrared Spectroscopy*, vol. 28, no. 4, pp. 186–203, 2020.

[11] Y. Wang, H. Huang, and X. Chen, "Predicting organic matter content, total nitrogen and ph value of lime concretion black soil based on visible and near infrared spectroscopy," *Eurasian Soil Science*, vol. 54, no. 11, pp. 1681–1688, 2021.

[12] H. P. Veeravu, S. Krishnapriya, G. Madhu, and D. K. Sahoo, "A statistical investigation into ammoniacal nitrogen adsorption on chitosan/bentonite nanocomposite films by response surface methodology," *Indian Journal of Environmental Protection*, vol. 39, no. 12, pp. 1106–1113, 2019.

[13] A. Alwi, R. Meder, Y. Japarudin, H. A. Hamid, R. Sanusi, and K. H. M. Yusoff, "Near infrared spectroscopy ofeucalyptus pellitafor foliar nutrients and the potential for real-time monitoring of trees in fertiliser trial plots," *Journal of Near Infrared Spectroscopy*, vol. 29, no. 3, pp. 158–167, 2021.

[14] A. O. Koroleva, T. A. Odintsova, M. Y. Tretyakov, O. Pirali, and A. Campargue, "The foreign-continuum absorption of water vapour in the far-infrared (50–500 cm1)," *Journal of Quantitative Spectroscopy and Radiative Transfer*, vol. 261, no. 5, Article ID 107486, 2021.

[15] I. Šestak, L. Mihaljevski Boltek, M. Mesić, Ž. Zgorelec, and A. Perčin, "Hyperspectral sensing of soil ph, total carbon and total nitrogen content based on linear and non-linear calibration methods," *Journal of Central European Agriculture*, vol. 20, no. 1, pp. 504–523, 2019.

[16] C. A. Andrade, L. A. Zambrano-Intriago, N. S. Oliveira, J. S. Vieira, L. S. Quiroz-Fernández, and J. M. Rodriguez-Diaz, "Adsorption behavior and mechanism of oxytetracycline on rice husk ash: kinetics, equilibrium, and thermodynamics of the process," *Water, Air, & Soil Pollution*, vol. 231, no. 3, p. 103, 2020.

[17] E. R. Thomson, M. P. Spiegel, I. H. J. Althuizen et al., "Multiscale mapping of plant functional groups and plant traits in the high arctic using field spectroscopy, uav imagery and sentinel-2a data," *Environmental Research Letters*, vol. 16, no. 5, Article ID 055006, 2021.

[18] X. Y. Li, P. P. Fan, Y. Liu, G. L. Hou, Q. Wang, and M. R. Lv, "Prediction results of different modeling methods in soil nutrient concentrations based on spectral technology," *Journal of Applied Spectroscopy*, vol. 86, no. 4, pp. 765–770, 2019.

[19] L. Zauska, S. Bova, E. Benova et al., "Thermosensitive drug delivery system sba-15-pei for controlled release of nonsteroidal anti-inflammatory drug diclofenac sodium salt: a comparative study," *Materials*, vol. 14, no. 8, p. 1880, 2021.

[20] X. Xu, L. Li, and A. Sharma, "Controlling messy errors in virtual reconstruction of random sports image capture points for complex systems," *International Journal of System Assurance Engineering and Management*, vol. 4, no. 3, 2021.

[21] M. Bradha, N. Balakrishnan, S. Suvi et al., "Experimental, computational analysis of Butein and Lanceoletin for natural dye-sensitized solar cells and stabilizing efficiency by IoT," *Environment, Development and Sustainability*, vol. 24, 2021.

[22] G. Vincenti, A. Bucciero, and C. Carvalho, "E-learning, E-education, and online training," *Lecture Notes of the*

Institute for Computer Sciences Social Informatics & Telecommunications Engineering, Springer, Berlin, Germany, 2014.

[23] X. Liu, C. Ma, and C. Yang, "Power station flue gas desulfurization system based on automatic online monitoring platform," *Journal of Digital Information Management*, vol. 13, no. 06, pp. 480–488, 2015.

[24] O. Issaoui, H. B. Amor, M. Ismail, L. Pirault-Roy, and M. R. Jeday, "Adsorption of bisphenol a from aqueous solution by hdtma-tunisian clay synthesized under microwave irradiation: a parametric and thermodynamic study," *Clays and Clay Minerals*, vol. 68, no. 4, pp. 361–372, 2020.

[25] R. Huang, S. Zhang, W. Zhang, and X. Yang, "Progress of zinc oxide-based nanocomposites in the textile industry," *IET Collaborative Intelligent Manufacturing*, vol. 3, no. 3, pp. 281–289, 2021.